Biochemistry and Biophysics Reports 2 (2015) 1–13

Contents lists available at ScienceDirect

Biochemistry and Biophysics Reports

journal homepage: www.elsevier.com/locate/bbrep

# Probing the role of aromatic residues in the self-assembly of Aβ(16–22) in fluorinated alcohols and their aqueous mixtures

Sanjai Kumar Pachahara, Ramakrishnan Nagaraj *

*CSIR-Centre for Cellular and Molecular Biology, Uppal Road, Hyderabad 500007, India*

ARTICLE INFO

*Article history:*
Received 6 March 2015
Received in revised form
16 April 2015
Accepted 17 April 2015
Available online 25 April 2015

*Keywords:*
Abeta peptide
Amyloid fibrils
Aromatic amino acids
Fluorinated alcohols
Self-assembly

ABSTRACT

The Aβ(16–22) sequence KLVFFAE spans the hydrophobic core of the Aβ peptide and plays an important role in its self-assembly. Apart from forming amyloid fibrils, Aβ(16–22) can self-associate into highly ordered nanotubes and ribbon-like structures depending on the composition of solvent used for dissolution. The Aβ(16–22) sequence which has FF at the 19th and 20th positions would be a good model to investigate peptide self-assembly in the context of aromatic interactions. In this study, self-assembly of Aβ(16–22) and its aromatic analogs obtained by replacement of F19, F20 or both by Y or W was examined after dissolution in fluorinated alcohols and their aqueous mixtures in solvent cluster forming conditions. The results indicate that the presence of aromatic residues Y and W and their position in the sequence plays an important role in self-assembly. We observe the formation of amyloid fibrils and other self-assembled structures such as spheres, rings and beads. Our results indicate that 20% HFIP is more favourable for amyloid fibril formation as compared to 20% TFE, when F is replaced with Y or W. The dissolution of peptides in DMSO followed by evaporation of solvent and dissolution in water appears to greatly influence peptide conformation, morphology and cross-β content of self-assembled structures. Our study shows that positioning of aromatic residues F, Y and W have an important role in directing self-assembly of the peptides.



## 1. Introduction

Interactions between aromatic amino acids play crucial roles in protein–protein recognition, ligand binding, structural stabilization and protein folding [1–6]. Interaction between the pairs of three aromatic amino acids F, Y and W in proteins have been documented extensively [6–8]. Stabilizing aromatic interactions have also been observed in short β-hairpin forming peptides [9–11]. However, these β-hairpin forming peptides do not self-associate. In self-assembling amyloidogenic peptides that have aromatic residues, they appear to play a role in the aggregation process [12–16]. While Aβ(16–22) has the FF pair, the β2m peptide is rich in F and Y [14]. Amyloidogenic peptides are not rich in W. The role of F in the self-assembly of short peptides has been studied extensively [12,15,17,18] but the roles of Y and W are poorly understood. The amino acids Y and W can stabilize β-hairpins in short peptides through stacking interactions [10,11]. Hairpin peptides with W–W and Y–Y cross-strand pairs that do not aggregate, prevent amyloid fibril formation in proteins [19]. It would be of interest to study the role of Y and W in the self-assembly of an amyloid forming sequence under amyloid fibril inducing and inhibiting conditions. Hexafluoroisopropanol (HFIP) has been used extensively to dissolve Aβ40, Aβ42 and other amyloidogenc peptides in order to ensure their monomeric status [20–25]. Low HFIP concentrations ( $\leq$ 10% v/v) in aqueous conditions promote amyloid fibril formation in Aβ and other amyloid peptides [26–29] whereas higher concentration of HFIP can inhibit fibril assembly or may dissociate pre-existing aggregates of Aβ [26,30]. The solvent trifluoroethanol (TFE) promotes the formation of α-helical and β-hairpin conformation in peptides [31,32]. TFE also induces amyloid fibril formation [27,33–35]. Water having 20% TFE promotes amyloid fibril formation in Aβ, α-synuclein and β2m peptide, presumably due to the presence of dynamic organic solvent clusters [27,33–35]. Mixtures of fluorinated alcohols and water can give useful insights in understanding aggregation pathways and intermediate structures of amyloid assembly in amyloidogenic proteins and peptides.

We have investigated how interaction between the aromatic residues F, Y and W modulate aggregation and morphology of aggregates in the well studied amyloidogenic peptide spanning residues 16–22 of Aβ40, Ac-KLVFFAE-amide (AβFF). We have systematically replaced F19, F20 and both the residues in Aβ(16–22) sequence with Y and W generating Ac-KLVFYAE-am (AβFY), Ac-KLVYFAE-am (AβYF), Ac-KLVYYAE-am (AβYY), Ac-KLVYWAE-am (AβYW), Ac-KLVWYAE-am (AβWY) and Ac-KLVWWAE-am (AβWW). We have examined the structures formed from solutions in HFIP

* Corresponding author. Tel.: +91 40 27192589; fax: +91 40 27160591/27160311.
*E-mail address:* nraj@ccmb.res.in (R. Nagaraj).

http://dx.doi.org/10.1016/j.bbrep.2015.04.005

and TFE and their 20% aqueous mixtures. In order to understand the effect of dissolution in dimethyl sulfoxide (DMSO), a solvent that prevents aggregation, self-assembly of peptides was investigated in deionized water after direct dissolution in water and dissolution of peptides dried from DMSO stocks.

## 2. Materials and methods

### 2.1. Materials

9-Fluorenylmethoxycarbonyl (Fmoc) protected amino acids were purchased from Advanced ChemTech (Louisville, KY, USA) and Novabiochem AG (Laufelfingen, Switzerland). Peptide synthesis resin, PAL resin (5-(4-aminomethyl-3,5-dimethoxyphenoxy) valeric acid resin), was purchased from Advanced ChemTech (Louisville, KY, USA). All other reagents and solvents were of highest grade available.

### 2.2. Peptide synthesis

Peptides were synthesized using standard Fmoc chemistry [36]. The N-terminus was acetylated [37]. The synthesized peptides were cleaved from the resin and deprotected using a mixture containing 82.5% TFA, 5% phenol, 5% $H_2O$, 5% thioanisole, and 2.5% ethanedithiol for 12–15 h at room temperature [38]. Peptides were precipitated in ice-cold diethyl ether and purified on Hewlett Packard 1200 series HPLC instrument on a reversed phase C18 Bio-Rad column using a linear gradient of $H_2O$ and acetonitrile (0–100% acetonitrile) containing 0.1% TFA. Purified peptides were characterized using matrix-assisted laser desorption/ionization time-of-flight mass spectrometry on an Applied Biosystem 4800 instrument at the Proteomics Facility of the Centre for Cellular and Molecular Biology, India. The observed and theoretical (shown in parentheses) $m/z$ values for peptides are as follows: AβFF: 894.57 (894.06), AβFY: 910.44 (910.06), AβYF: 910.43 (910.06), AβYY: 926.41 (926.06), AβYW: 949.40 (949.06), AβWY: 949.39 (949.06), and AβFY: 972.39 (972.06). After purification, the solvent ($H_2O$–acetonitrile mixture containing 0.1% TFA) was evaporated and the peptides were stored as dry solids. Peptide stock solutions were prepared from the dried solids in HFIP, TFE and DMSO. Concentrations were estimated by diluting the peptides in the respective solvents. The concentrations of peptides were calculated using the molar absorption coefficients of 1280, and 5690 $M^{-1}\,cm^{-1}$ at $\lambda = 280$ nm for Y and W, respectively. For AβFF, a molar absorption coefficient of 286 $M^{-1}\,cm^{-1}$ was used at 254 nm.

### 2.3. Peptide solutions

All peptide solutions in HFIP and TFE were at a concentration of 1.2 mM. These stock solutions were diluted 5-fold in deionized water to ensure same concentrations for all the peptides in both the aqueous organic mixtures *i.e.* 20% HFIP and 20% TFE. Similarly, peptide solutions were prepared in DMSO at 1 mM concentrations and solvent was dried in speed vac concentrator. Peptides treated with DMSO and HPLC purified peptides without DMSO treatment were dissolved in deionized water at 0.5 mM concentration.

### 2.4. Atomic force microscopy

Stock solutions of peptides prepared in HFIP and TFE at 1.2 mM concentration were incubated for two weeks at 25 °C to effect complete dissolution prior to AFM imaging. Peptides (2 μl) were deposited on freshly peeled mica surfaces from HFIP and TFE stocks, and air dried prior to imaging. If aggregates were very dense, peptides were diluted appropriately (2–5 fold) in the same solvent and deposited immediately. The images were acquired using tapping mode AFM (Hydra SPM MultiView 4000, Nanonics Imaging Ltd., Jerusalem, Israel). A glass probe of 10 nm diameter was oscillated at ~34 kHz and images were collected at an optimized scan rate of 5 ms per dot. Images were recorded as $512 \times 512$ dots per image in $X$ and $Y$ dimension. Analysis was done using WSxM v5.0 Develop 6.3 [39]. All the images were flattened and presented in the height mode.

### 2.5. Transmission electron microscopy

Peptides dissolved in organic solvents (TFE and HFIP) at 1.2 mM concentration were diluted 5-fold in deionized water (20% organic solvent) and imaged immediately after dilution and after 10 days of incubation at 25 °C. Peptides dissolved in deionized water were imaged after one month incubation at room temperature. Peptide solutions were placed on a carbon-coated Formvar 200-mesh copper grid. After 2 min, solvent was blotted out by touching the Whatman filter paper at peripheral part of the grids. Then, grids were stained with saturated uranyl acetate solution which was blotted out after 30 s. Images were captured using JAM-2100 LaB6 transmission electron microscope (JEOL, Tokyo, Japan) at 100 kV. Dimension measurements of structures were done with the help of software digital micrograph (Gatan, Inc.).

### 2.6. Thioflavin T fluorescence spectroscopy

Thioflavin T (ThT) fluorescence spectra were recorded on Fluorolog-3 Model FL3-22 spectrofluorometer (Horiba Jobin Yvon, Park Avenue Edison, NJ, USA). ThT spectra of samples were recorded in 10 μM ThT solution in 10 mM phosphate buffer pH 7.4. Briefly, peptide solutions were diluted to 10 μM peptide concentrations in 10 μM ThT solution in 10 mM phosphate buffer pH 7.4. Blank ThT spectra were recorded by adding same volumes of cosolvents in 10 μM ThT solution in 10 mM phosphate buffer pH 7.4. The excitation wavelength was set at 450 nm, slit width at 2 nm, and emission slit width at 5 nm.

### 2.7. CD spectroscopy

Far-UV CD spectra of the peptides were recorded on a Jasco J-815 spectropolarimeter (Jasco, Tokyo, Japan). Spectra were recorded at a concentration of 100 μM. All the spectra were recorded in 0.1 cm path length cell using a step size of 0.2 nm, band width of 1 nm, and scan rate of 100 nm $min^{-1}$. The spectra were recorded by averaging eight scans and corrected by subtracting the solvent spectra. Mean residue ellipticity (MRE) was calculated using the formula: $[\theta]\mathrm{MRE} = (\mathrm{Mr} \times \theta\,\mathrm{mdeg})/(100 \times l \times c)$, where Mr is mean residue weight, $\theta$ mdeg is ellipticity in millidegrees, $l$ is path length in decimeter, and $c$ is the peptide concentration in mg $ml^{-1}$.

### 2.8. Fourier transform IR spectroscopy

FTIR spectra were recorded on a Bruker Alpha-E spectrometer (Bruker Optik GmbH, Ettlingen, Germany) with Eco attenuated total reflection (ATR) single reflection ATR sampling module equipped with ZnSe ATR crystal. Peptides were spread out and dried as films on ZnSe crystal and ATR-FTIR spectra were recorded. Each spectrum is the average of 64 FTIR spectra at a resolution of 4 $cm^{-1}$. All the spectra were normalized to the scale of zero to one arbitrary absorbance unit to facilitate easy comparison.

## 3. Results

### 3.1. Aggregation from HFIP and TFE solutions

Peptides AβFF, AβFY, AβYF, AβYY, AβYW, AβWY, and AβWW dissolved in HFIP at 1.2 mM concentration were imaged by AFM. When highly dense structures from stock solutions were observed, peptide solutions were diluted appropriately (2–5-fold) in the same solvent prior to deposition over freshly peeled mica surface. Stock solutions of AβFF, AβFY, AβYF and AβYY were diluted 5-fold. AβYW and AβWY were diluted 2-fold and AβWW was not diluted prior to their deposition on mica surface. Fig. 1 shows the AFM images of structures formed when peptides were dried from HFIP stock solutions. Panels A–G represent the images recorded from the peptides AβFF, AβFY, AβYF, AβYY, AβYW, AβWY, and AβWW, respectively. Height profiles of structures shown below the images represent the structures that come on the black line in the image. Black lines and height profiles were generated using the "profile" tool in WSxM 5.0 software. AβFF self-associates into spherical aggregates of 4–20 nm height. Small spherical aggregates (~4 nm, indicated by arrows) were associated with large spheres (10–20 nm) giving an eyeball-like appearance (Panel A). The spherical structures of both sizes were also present in isolation. Similar eyeball-like structures of $133 \pm 43$ nm diameter along with smaller spheres ($51 \pm 43$), interpreted as molten particles, were reported for AβFF in 60% methanol (0.1% TFA) at 4 °C [40]. AβFY forms globular and amorphous structures of 3–6 nm height (Panel B). AβYF self-assembles into polymorphic structures that are spherical or spindle shaped aggregates of 10–20 nm height and short cigar-like aggregates (indicated by arrows) of 2–3 nm height (Panel C). Magnified image of short cigar-like structures ( < 500 nm in length) is shown in inset in panel C. AβYY forms bead-like linear aggregates of 4–10 nm heights Few cigar-like aggregates of 2–3 nm height were also present (indicated by arrows in panel D). AβYW self-associates into polymorphic structures. Oligomeric structures of 2–4 nm height, spherical structures of 8–20 nm height and annular structures of 6–12 nm height were observed (Panel E). Annular structures appear to be formed by association of short fibrillar structures with tapering ends. Annular structures are indicated by arrows in panel E. AβWY self-associates into ring-like structures of two distinct sizes, larger rings are of 6–8 nm height and 0.5–0.8 μm diameter whereas small rings are of ~2 nm height and 0.2–0.3 μm diameter (Panel F). Small rings are indicated by arrows and a magnified imaged of 1 μm × 1 μm is shown in inset (panel F). Ring-like structures resulted from the self-assembly of AβWW are of 4–10 nm height and 0.25–0.8 μm diameter (Panel G), a magnified imaged of 1 μm × 1 μm is shown in inset. We have reported similar ring-like structures for Aβ(1–40), Aβ(1–42), Aβ(1–43) and Aβ(16–22) peptides [41] upon drying from HFIP stocks. Morphology of the aggregated structures formed after dissolution in HFIP is dependent on the nature of aromatic amino acids in positions 19 and 20 of the Aβ(16–22) sequence.

Fig. 2 shows the AFM images of structures formed when peptides were dried from TFE stock solutions (1.2 mM). Peptide stock solutions were diluted 5-fold prior to deposition (2 μl of diluted sample) on mica surface except for AβFY and AβYW peptide (without any dilution). Panels A–G represent the images recorded from the peptides AβFF, AβFY, AβYF and AβYY, AβYW, AβWY, and AβWW, respectively. AβFF self-assembles into globular aggregates of height range 5–15 nm (Panel A). Peptide AβFY forms 1–5 μm long thick fibrillar structures of 8–12 nm height (Panel B). These thick fibrillar structures appear to form by lateral association or twisting of thin (2–4 nm height) fibrillar structures. Twisting of thin fibrillar structures and their lateral association are shown by black and white arrows respectively (Panel B). Fibrillar structures of 2–10 nm height and 1–3 μm length were observed in case of AβYF (Panel C). AβYY self-associates into linear

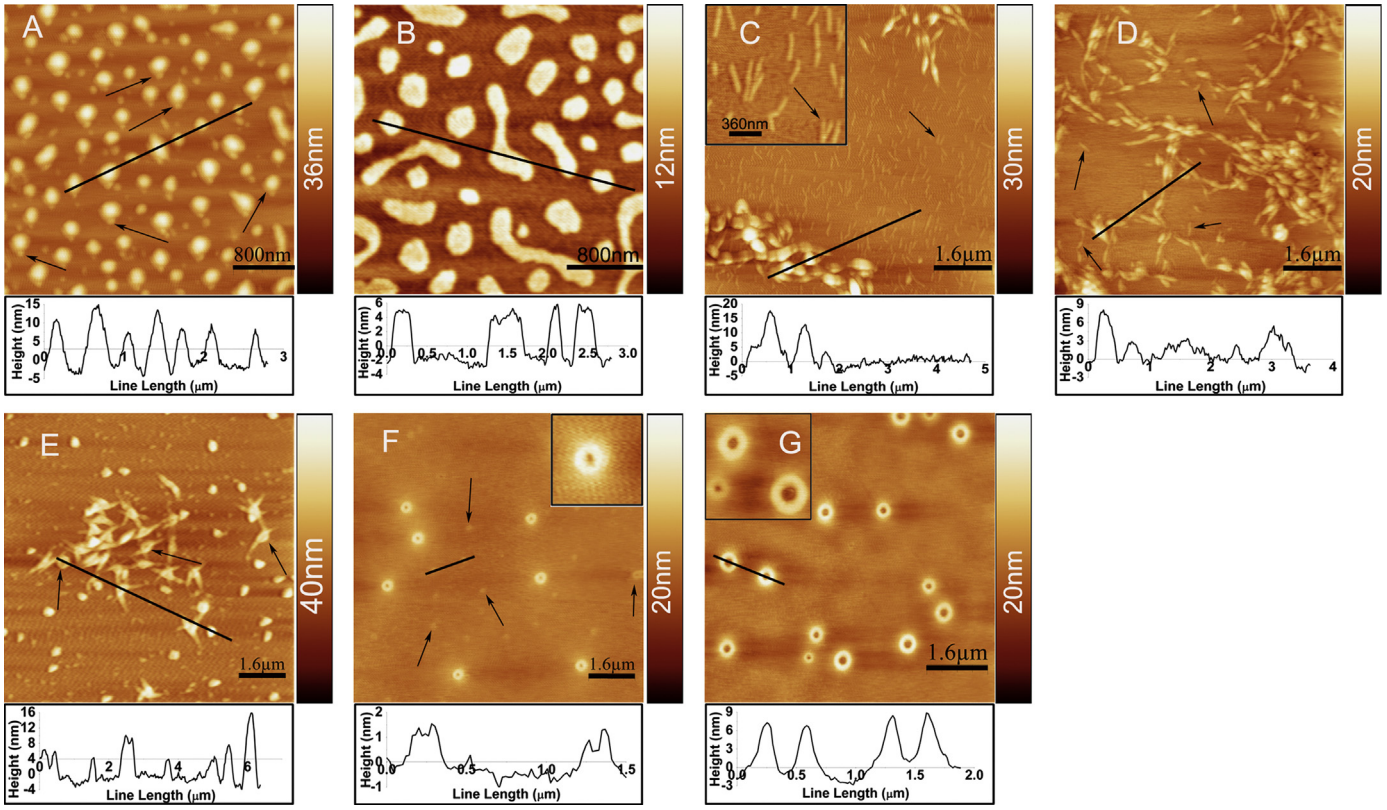


**Fig. 1.** AFM images of peptide structures formed upon drying from HFIP stock solutions. Panels A–G represent the images recorded from the peptides AβFF, AβFY, AβYF, AβYY, AβYW, AβWY, and AβWW, respectively. A magnified image of 1 μm × 1 μm is shown in inset of panels F and G. Height profile of the structures present under the black lines is shown under the respective images.

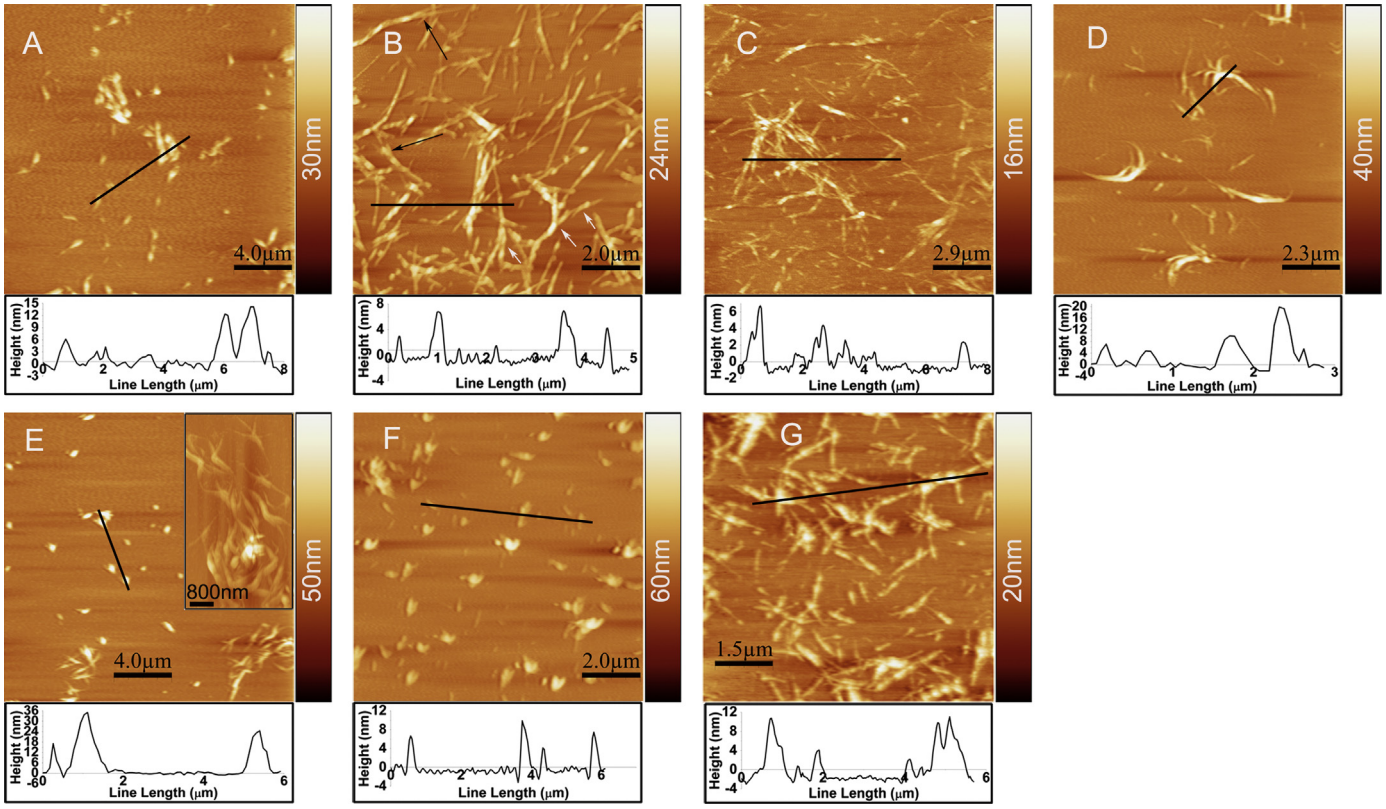


**Fig. 2.** AFM images of peptide structures formed upon drying from TFE stock solutions. Panels A–G represent the images recorded from the peptides AβFF, AβFY, AβYF, AβYY, AβYW, AβWY, and AβWW, respectively. Height profile of the structures present under the black lines is shown under the respective images.

and curved fibrils of 5–10 and 10–20 nm heights, respectively (Panel D). Curved fibrils have tapering ends and are relatively longer (2–4 μm) than linear structures (1–2 μm). AβYW self-assembles into globular aggregates of 10–40 nm height (Panel E) and fibrillar aggregates of 5–15 nm height (Panel E, shown in inset). Peptide AβWY forms amorphous structures (Panel F). AβWW self-associates into protofibrillar structures of 3–6 nm height (Panel G).

### 3.2. Aggregation of peptides in aqueous mixtures of organic solvents

Aggregation behaviour from aqueous solutions was examined by Transmission electron microscopy and ThT fluorescence spectroscopy. Peptides, freshly dissolved in organic solvents (HFIP and TFE), were diluted into deionized water (1:4 v/v) and imaged immediately after dilution and after 10 days of incubation at 25 °C. Peptides imaged from aqueous HFIP stocks at both the time points are shown in Fig. 3. AβFF does not form distinctive structures immediately after dilution from HFIP stock (Panel A). After 10 days of incubation, short fibrillar structures of 150–600 nm length and 15–25 nm diameter were observed. Fibrils originating from globular structures are shown by arrows in panel B. Apart from short fibrillar structures, several micrometers long bundles of fibrillar structures (30–80 nm thick) that appear to form by association of thinner fibrils (8–12 nm) were also observed (shown in inset in panel B). Structures observed for AβFF show very poor enhancement of ThT fluorescence (shown as bars next to panel B) indicating that the structures are not amyloidogenic. AβFY, self-assembles into fibrillar structures with width range in between 10 and 200 nm (Panel C) immediately after dilution from HFIP. After incubation, dense aggregates of fibrillar structures were observed (Panel D). Fibrils formed by AβFY are amyloid in nature as suggested by significant ThT fluorescence enhancement (shown as bars next to panel D). Freshly diluted AβYF self-assembles into several micrometers long ribbon-like structures of 40–100 nm width with irregular twists at 200–800 nm (Panel E). After incubation, ribbon-like structures associate loosely to form higher order structures (rod-like structures of 20–60 nm thickness and 0.2–2 μm length, Panel F). The ribbon-like structures (50–150 nm width and 0.2–2 μm length) were also observed in isolation (inset in panel F). AβYY self-assembles into spherical aggregates of 10–40 nm diameter, and fibrils of less than one μm length and 8–16 nm thickness from freshly diluted stock (Panel G). Fibrils and spherical structures were found in isolation and in close association with each other. At a few places, very large fibrillar structures (several micrometers long and 70–200 nm thick) were observed. These fibrillar aggregates appear to be formed by loose association of thin fibrils (inset in panel G). After incubation, all the spherical structures disappear and very large fibrillar structures (several micrometers long and 70–200 nm thick) emerge that are clearly visible to be formed by loose association of thin fibrils (10–20 nm thickness) (Panel H). Structures observed for AβYF and AβYY show moderate enhancement in ThT fluorescence intensity as compared to AβFY (shown as bars next to panels F and H, respectively). Self-assembled structures from AβYW appeared amorphous when imaged immediately after dilution from HFIP stock or after 10 days of incubation (Panels I and J, respectively). AβWY self-assembles into fibrillar structures of ~10 nm thickness and 0.2–0.8 μm length (Panel K, immediately after the solution is prepared). The fibrillar structures dissociate and amorphous aggregates were observed after 10 days of incubation (Panel L). Structures observed for AβYW and AβWY show enhancement in ThT fluorescence intensity (shown as bars next to panels J and L, respectively) comparable to AβYF and AβYY. AβWW self-assembles into spherical aggregates of 100–200 nm diameter and amorphous structures in freshly diluted solution (Panel M)

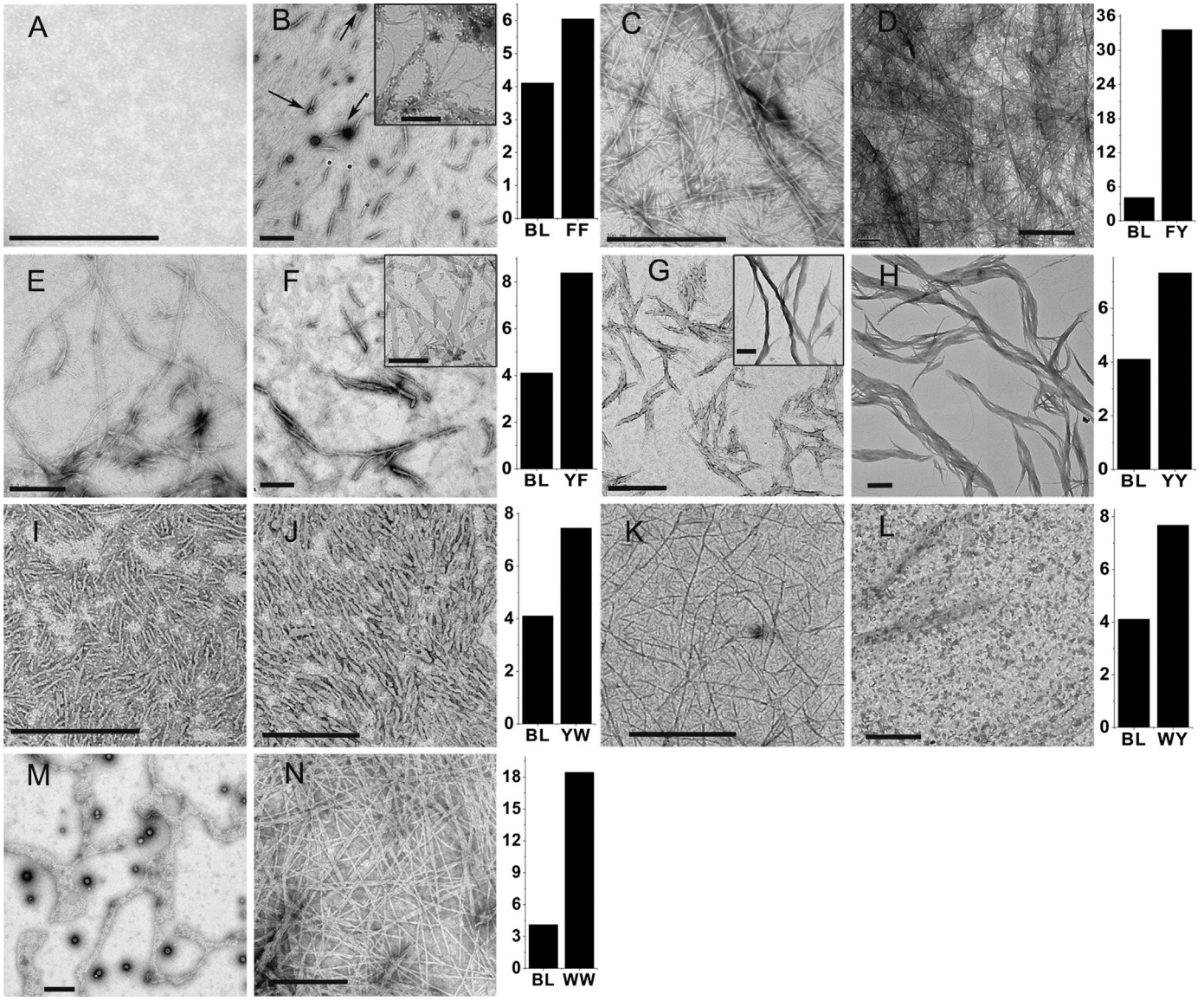


**Fig. 3.** TEM images and ThT fluorescence spectroscopy of peptides dissolved in 20% HFIP. Images recorded from freshly prepared and 10 days incubated solutions are shown in panels A and B, C and D, E and F, G and H, I and J, K and L, and M and N, respectively for the peptides AβFF, AβFY, AβYF, AβYY, AβYW, AβWY, and AβWW, respectively. Scale bars correspond to 500 nm. Enhancements in ThT fluorescence at 482 nm are shown with the images recorded from 10 days incubated peptide stocks. Intensities of ThT fluorescence (AU) at 482 nm were taken from ThT fluorescence spectra recorded from 10 days incubated stocks. BL (blank) represents ThT fluorescence intensity in buffer in absence of peptide and corresponding fluorescence intensities in presence of peptide are presented for easier comparison.

whereas fibrils of 20–100 nm thickness and several micrometers length were observed (Panel N) after 10 days of incubation. Fibrils formed by AβWW are amyloid in nature as suggested by significant ThT fluorescence enhancement.

Peptides were imaged immediately after dilution of TFE stocks into deionized water and after 10 days incubation of diluted stocks at 25 °C. TEM imaging from aqueous TFE stocks at both the time points is shown in Fig. 4. AβFF initially forms well defined spherical aggregates (30–50 nm diameter) and weakly stained fibrillar structures (8–12 nm thickness and ~200 nm long) (Panel A). Upon incubation, short fibrillar structures (Panel B, indicated by arrows) form dense clusters which show enhancement in ThT fluorescence. AβFY self-associates into several micrometers long rod-like structures of 10–100 nm width (Panel C). Irregular twists spaced by 100–500 nm length are observed (Panel C, indicated by arrows) in some of the structures. After incubation, several micrometers long distinct fibrillar structures of 10–30 nm thickness are observed (Panel D). Distinctly visible fibrils formed by AβFY showed intense ThT fluorescence as compared to clusters of fibrillar structures observed for AβFF (shown as bars next to panels B and D). AβYF formed helical ribbons of sub-micrometer to several micrometers length and 15–90 nm width with a twist periodicity of ~100–300 nm (Panel E). Apart from helical ribbons, disc-shaped structures of 10–60 nm diameter and thin fibrillar structures (8–12 nm thickness) of less than a micrometer length were also observed from freshly prepared solution. An arrow shows origin of thin fibril from a disc (Panel E). After incubation, the discs disappeared completely and both twisted ribbons along with flat fibrils of several micrometers lengths were observed (Panel F). The fibrillar structures were broader (50–110 nm, indicated by arrows in panel F) compared to the twisted ribbons with periodic twists (20–50 nm), twists repeated after an interval of 300–500 nm. A magnified image of twisted ribbons is shown as inset in panel F. AβYY forms rod-like structures of 10–15 nm diameter and sub-micrometer length (Panel G, indicated by arrows) aggregated to form dense sheet-likes structures when imaged immediately after preparation of solution. Upon incubation, structures appear to disintegrate (Panel H). Structures formed

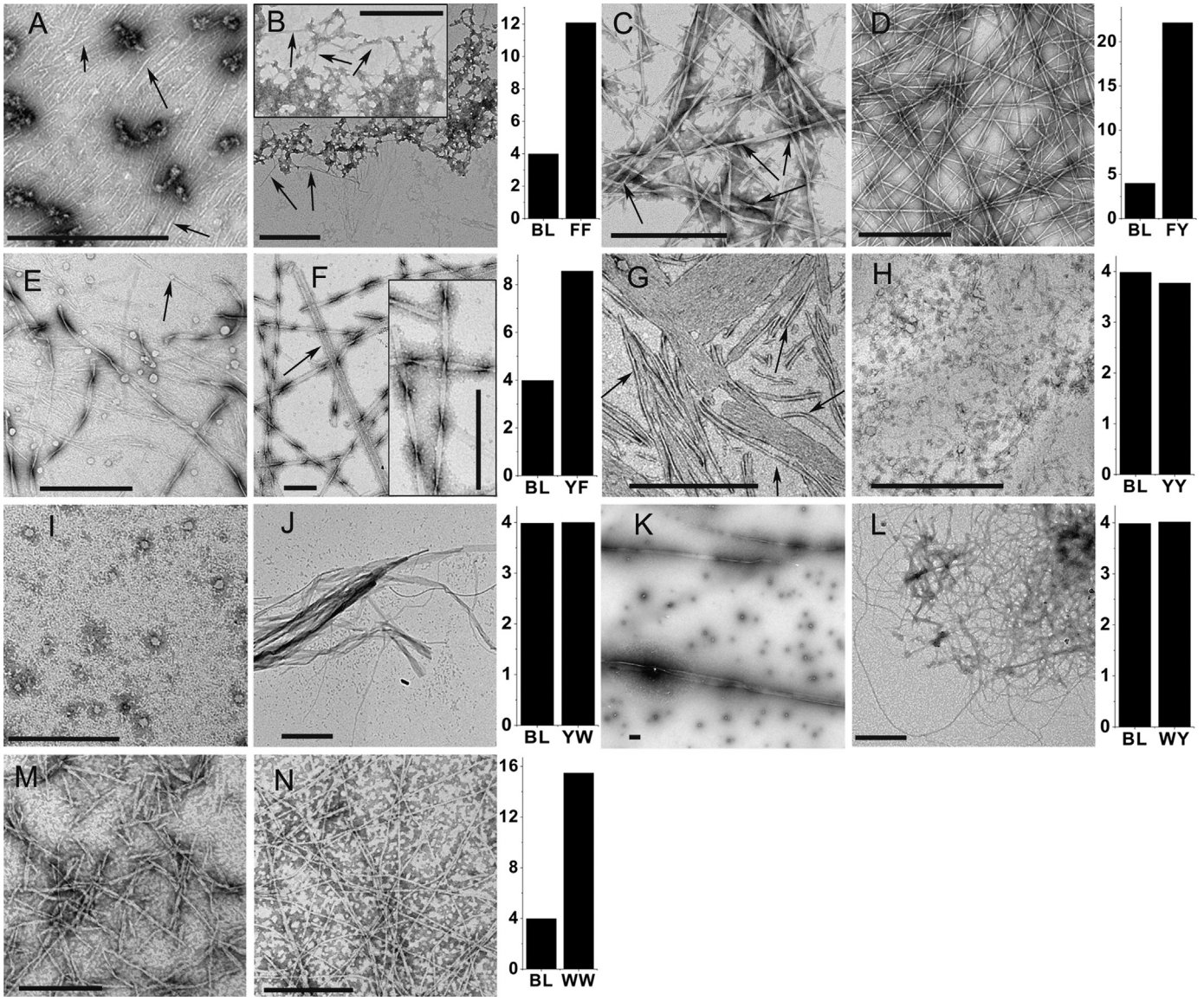


**Fig. 4.** TEM images and ThT fluorescence spectroscopy of peptides dissolved in 20% TFE. Images recorded from freshly prepared and 10 days incubated solutions are shown in panels A and B, C and D, E and F, G and H, I and J, K and L, and M and N, respectively for the peptides AβFF, AβFY, AβYF, AβYY, AβYW, AβWY, and AβWW, respectively. Scale bars correspond to 500 nm. Enhancements in ThT fluorescence at 482 nm are shown with the images recorded from 10 days incubated peptide stocks. Intensities of ThT fluorescence (AU) at 482 nm were taken from ThT fluorescence spectra recorded from 10 days incubated stocks. BL (blank) represents ThT fluorescence intensity in buffer in absence of peptide and corresponding fluorescence intensities in presence of peptide are presented for easier comparison.

by AβYF are amyloid in nature as suggested by significant ThT fluorescence enhancement whereas structures formed by AβYY are not amyloid-like (shown as bars next to panels F and H, respectively). AβYW initially forms spherical (30–50 nm diameter) and amorphous aggregates (Panel I). Upon incubation, ribbon-like structures of 20–200 nm width and several micrometers length were observed (Panel J). AβWY forms spherical structures (100–200 nm diameter), few very broad and long (200–400 nm width and several micrometers long) ribbon-like structures were also observed from freshly diluted stock (Panel K). Upon incubation, several micrometers long fibrils of 10–20 nm diameters were observed (Panel L). Ribbon-like structures and fibrils observed for AβYW and AβWY respectively, are not amyloids as they do not show ThT fluorescence enhancement. (shown as bars next to panels J and L, respectively). From a freshly prepared solution, AβWW self-assembles into fibrillar structures that resemble protofibrils of 20–40 nm thickness and 200–800 nm length (Panel M). Upon incubation, several micrometers long mature fibrils of 10–20 nm thickness were observed (Panel N). AβWW fibrils are amyloid in nature as suggested by significant ThT fluorescence enhancement (bars shown next to panel N).

### 3.3. Aggregation of peptides in deionized water after direct dissolution and dissolution after DMSO treatment

In order to examine the impact of dissolution in DMSO on the self-assembly of peptides, the aggregation behaviour of peptides was examined in deionized water. HPLC purified peptides were dissolved directly in water (DMSO untreated) and peptides dissolved in DMSO were dried and dissolved in water (DMSO treated). Images recorded after one month incubation of DMSO untreated and treated peptides dissolved in water are shown in Fig. 5. Panels A and B represent images recorded from DMSO untreated and treated AβFF solutions, AβFF forms fibrils of ~0.2–4 μm length and ~10–30 nm in thickness (Panel A). DMSO treated stock of AβFF shows polymorphic structures composed of fibrils and ribbons. The dimensions of the structures are of 30–130 nm width and lengths ranging from 0.3 to several micrometers (Panel B). Enhancement in

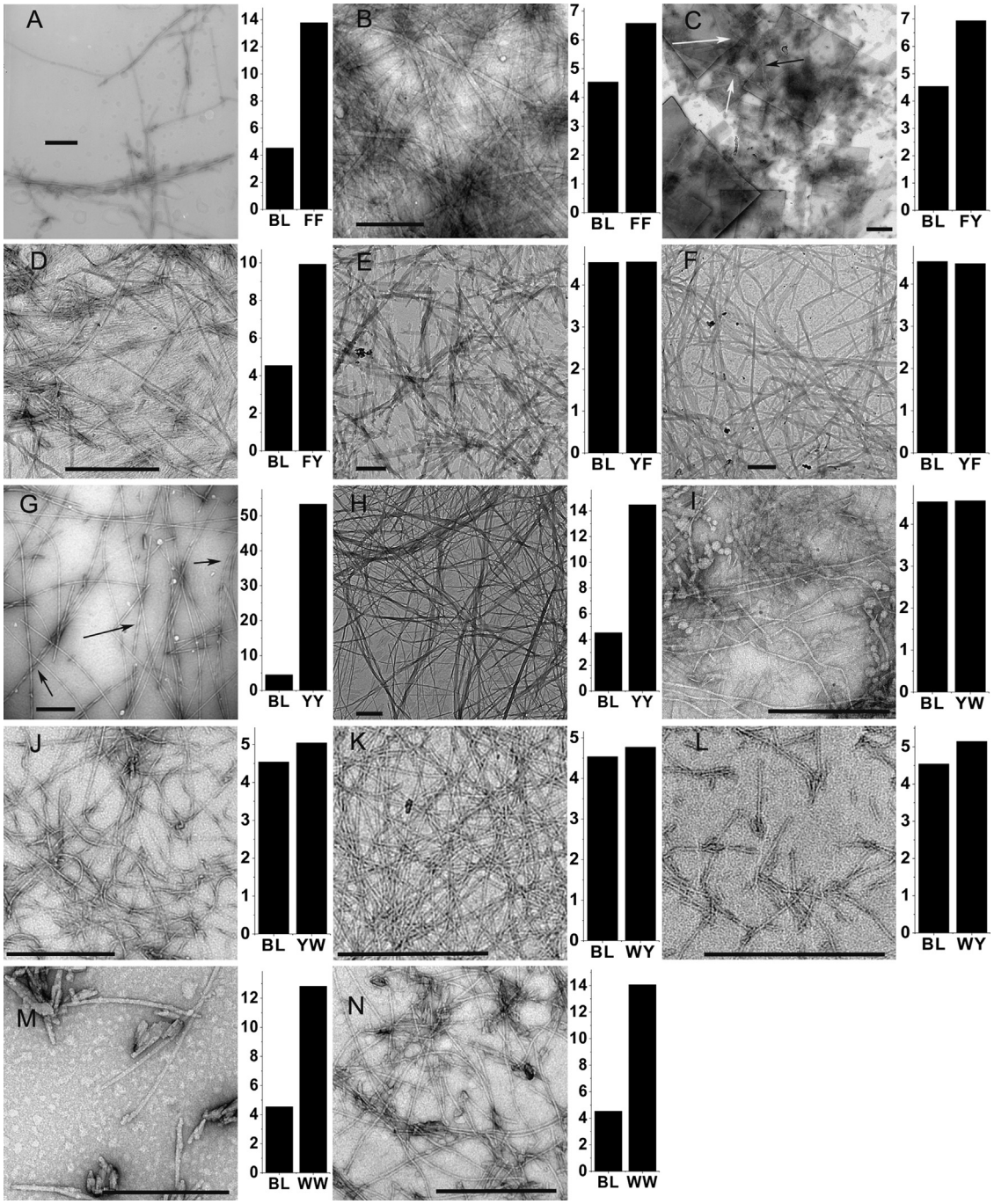


**Fig. 5.** TEM images and ThT fluorescence spectroscopy of peptides dissolved in deionized water directly or after DMSO treatment. Images recorded from one month incubated solutions are shown in panels A and B, C and D, E and F, G and H, I and J, K and L, and M and N, respectively for the peptides AβFF, AβFY, AβYF, AβYY, AβYW, AβWY, and AβWW, respectively. Scale bars correspond to 500 nm. Enhancements in ThT fluorescence at 482 nm are shown with the corresponding images. Intensities of ThT fluorescence (AU) at 482 nm were taken from ThT fluorescence spectra recorded from one month incubated stocks. BL (blank) represents ThT fluorescence intensity in buffer in absence of peptide and corresponding fluorescence intensities in presence of peptide are presented for easier comparison.

ThT fluorescence is significantly less from DMSO treated peptide as compared to DMSO untreated stock (bars next to panels A and B). The structures observed from aqueous solution after DMSO treatment could be largely nanotubes interspersed with amyloid fibrillar structures. AβFY forms square or rectangular sheets of 0.5–4 μm dimensions with few fibrils of 0.2–1 μm length and 8–20 nm width (fibrils are indicated by arrows, panel C). DMSO treated AβFY forms fibrils of 0.2 to several micrometers length and 8–20 nm thickness (panel D). The fibrillar structures present in panel C cause a small enhancement in ThT fluorescence whereas fibrils formed from DMSO treated peptide showed relatively greater ThT fluorescence (bars next to panels C and D). AβYF self-assembles to form 50–100 nm broad tape-like structures of several micrometers length in both DMSO untreated and treated conditions (panels E and F, respectively). Tape-like structures of AβYF from both the conditions do not show enhancement in ThT fluorescence. AβYY forms cylindrical fibrils of several micrometers length and 20–40 nm width, some fibrils of similar dimensions having regular twists of about 150–200 nm were also present (indicated by arrows, panel G) without DMSO treatment. On DMSO treatment AβYY shows flat fibrils of 40–140 nm width (significantly broader than DMSO untreated) and several micrometers in

length (Panel H). AβYY fibrils from DMSO untreated peptide showed intense ThT fluorescence whereas AβYY fibrils from DMSO treated peptide showed relatively poor enhancement of ThT fluorescence.

AβYW forms several micrometers long fibrils of 10–20 nm thickness from both DMSO untreated and treated stocks (Panels I and J, respectively). AβWY also forms long fibrils of 10–20 nm thickness from DMSO untreated stock (Panel K) whereas on DMSO treatment the peptide self-associates into fibrillar structures of 10–20 nm thickness and 100–800 nm length (Panel L). Fibrillar structures formed by AβYW and AβWY from DMSO untreated/ treated peptides dissolved in deionized water are not amyloid in nature as indicated by absence of enhancement in ThT fluorescence. AβWW self-associates into thick (20 nm) fibrillar structures of 200–800 nm length from DMSO untreated stock (Panel M). Several micrometers long fibrils of 10–15 nm thickness were observed from DMSO treated stock of AβWW (panel N). Fibrils formed by AβWW from both DMSO untreated/ treated peptides dissolved in deionized water are amyloids as significant enhancement in ThT fluorescence was observed.

The self-assembled structures observed from peptides directly dissolved in deionized water and dissolved after DMSO treatment are considerably different. Apart from morphological differences, differences in the enhancement of ThT fluorescence are also evident for DMSO treated and untreated peptides. The position of F and Y determine morphology of the structures. While AβFY favours fibril formation when dissolved in water (DMSO treated), AβYF form tape-like structures which do not have cross-β structure. Fibril forming propensity from water is greatest for the AβYY sequence. Structures observed from W-containing peptides directly dissolved in deionized water and dissolved after DMSO treatment have only subtle morphological differences which can be attributed to differences in conformation and/or side-chain packing. Fibrils were formed by all the peptides irrespective of DMSO treatment. The amyloid nature of fibrils in W containing peptides is not dependent on DMSO pre-treatment unlike AβFF, AβFY, and AβYY.

### 3.4. CD spectroscopy

Far UV CD spectra of peptides dissolved in TFE, HFIP and their dilutions into deionized water (20% organic solvent) were recorded after 2 weeks of incubation at 25 °C. CD spectra of the peptides in the different solvents are shown in Fig. 6. In HFIP and TFE, AβFF shows a positive band centred around 195 nm. A negative band centred at 212 nm with low intensity was observed only in HFIP. In 20% HFIP, a positive band around 192 nm was observed (Panel A). Positive ellipticity bands at 197–200 nm and 218–220 observed in diphenylalanine containing peptides have been assigned to $\pi$–$\pi^*$ and n–$\pi^*$ aromatic side-chain electronic transitions, respectively [42–44]. Red shift was reported in CD spectra characteristic of β-sheet conformation peaks (positive peak at 195 nm shifted to 200 nm and negative peak at 216 nm shifted to 226 nm) for Aβ(16–22) peptide [45]. In TFE, AβFF shows a broad minimum at ~215–235 nm, an indicative of β-structure. CD spectrum of AβFY in TFE indicates β-conformation (Panel B). Spectra recorded in 20% HFIP suggest the presence of both α-helix and β-structure. In 20% TFE, AβFY adopts β-structure (Panel B). The spectrum of AβYF in 20% TFE shows a prominent negative band that is red-shifted by 5–10 nm from bands characteristic of β-sheet conformation (Panel C). Red-shift of the band in CD spectra as a result of strong aromatic stacking was also evident in Aβ(16–22) peptide [45]. In 20% HFIP, the spectrum of AβYF indicates presence of α-helical conformation (Panel C) which could arise due to structural heterogeneity of aggregates. In 20% HFIP, the spectrum of AβYY is characteristic of α-helical conformation (Panel D). CD spectra of AβYW in HFIP and TFE show negative bands at ~220 nm (Panel E). Negative ellipticty at ~220 nm can be attributed to indole $B_b$ transitions [46]. In 20% HFIP, a minimum at ~205 nm and shoulder at ~220 nm is indicative of α-helical conformation (Panel E). The spectra of AβWY shows a prominent negative band at ~200 nm and cross-over at ~195 nm in TFE and HFIP. In 20% HFIP, the double minima are characteristic of helical conformation (Panel F). The spectra of AβWW show a prominent negative band at ~220 nm in HFIP, TFE and 20% HFIP. In 20% TFE, two negative bands at ~210 and 220 nm of comparable intensities are observed (Panel G). The spectrum indicates multiple conformations. While contributions from aromatic residues can distort CD spectra, it is evident that the peptides tend to adopt ordered conformation in the solvents examined except for AβYF and AβYY which show ordered conformation only in aqueous condition containing 20% HFIP or TFE.

CD spectra of peptides dissolved in deionized water (with or without DMSO treatment) were recorded within 36 h of dissolution. CD spectra are shown in Fig. 7. Spectra of DMSO untreated peptides are represented by continuous lines whereas spectra from DMSO treated peptides are shown by dotted lines. CD spectra of AβFF in both the conditions appear to be largely unordered (Panel A). AβFY shows intense positive bands at 200 nm under both the conditions indicating $\pi$–$\pi^*$ transitions (Panel B). The intensity of the bands suggests conformational differences between DMSO treated and untreated samples. CD spectra of AβYF in deionized water (both DMSO treated and untreated) show negative bands at lower wavelengths suggesting largely unordered structure (Panel C). CD spectra of AβYY peptide are completely different in both the conditions. DMSO untreated stock shows a negative band at ~215 nm with low intensity indicating β-structure whereas peptide from DMSO treated stock is characteristic of unordered conformation [47] (Panel D). The spectra of AβYW are characteristic of unordered conformation under both the conditions (Panel E). AβWY shows a broad negative band at ~215 nm in both the conditions suggesting β-structure (Panel F). Positive elipticity at 226–230 nm could possibly result from Y side-chains [48–50]. AβWW shows negative bands at ~210 nm and a negative band at ~230 nm with lower intensity (Panel G) under both the conditions. The band at ~230 nm could arise due to interaction between W residues as observed in Indolicidin, a W rich antimicrobial peptide [51], and a model cyclic peptide rich in W [52].

### 3.5. FTIR spectroscopy

Amide I region in FTIR spectra is sensitive to secondary structures of proteins and peptides as it arises from C=O stretching vibration with a small admixture of the NH bending [53]. The peptides were dried on ZnSe crystal from different solvents and ATR–FTIR spectra of dry peptide films were recorded to correlate the peptide secondary structures in the solid state. For easier comparison of peaks, spectra were normalized to a scale of 0–1.0. Spectra are shown in Fig. 8. Peptides AβFF and AβFY show sharp peaks in amide I region centered at 1626 $cm^{-1}$ upon drying from HFIP stocks. Peptide solutions dried from TFE, 20% HFIP and TFE in water, are centred at 1625 $cm^{-1}$ (Panels A and B, respectively). Amide I bands at about 1615–1630 $cm^{-1}$ have been assigned to β-structure of amyloid fibrils [54]. AβFF structures formed in HFIP and deionized water show significant intensity at 1660–1680 $cm^{-1}$ which could arise due to TFA salt. A high frequency and low intensity band at about 1685–1695 $cm^{-1}$ has been assigned to non-fibrillar structures of several proteins and this band disappears upon fibrillation [54]. A low intensity band centered at about 1690 $cm^{-1}$ for the structures formed by AβFY in all the conditions could possibly result from non-fibrillar structures (Panel B). AβYF shows relatively broader band

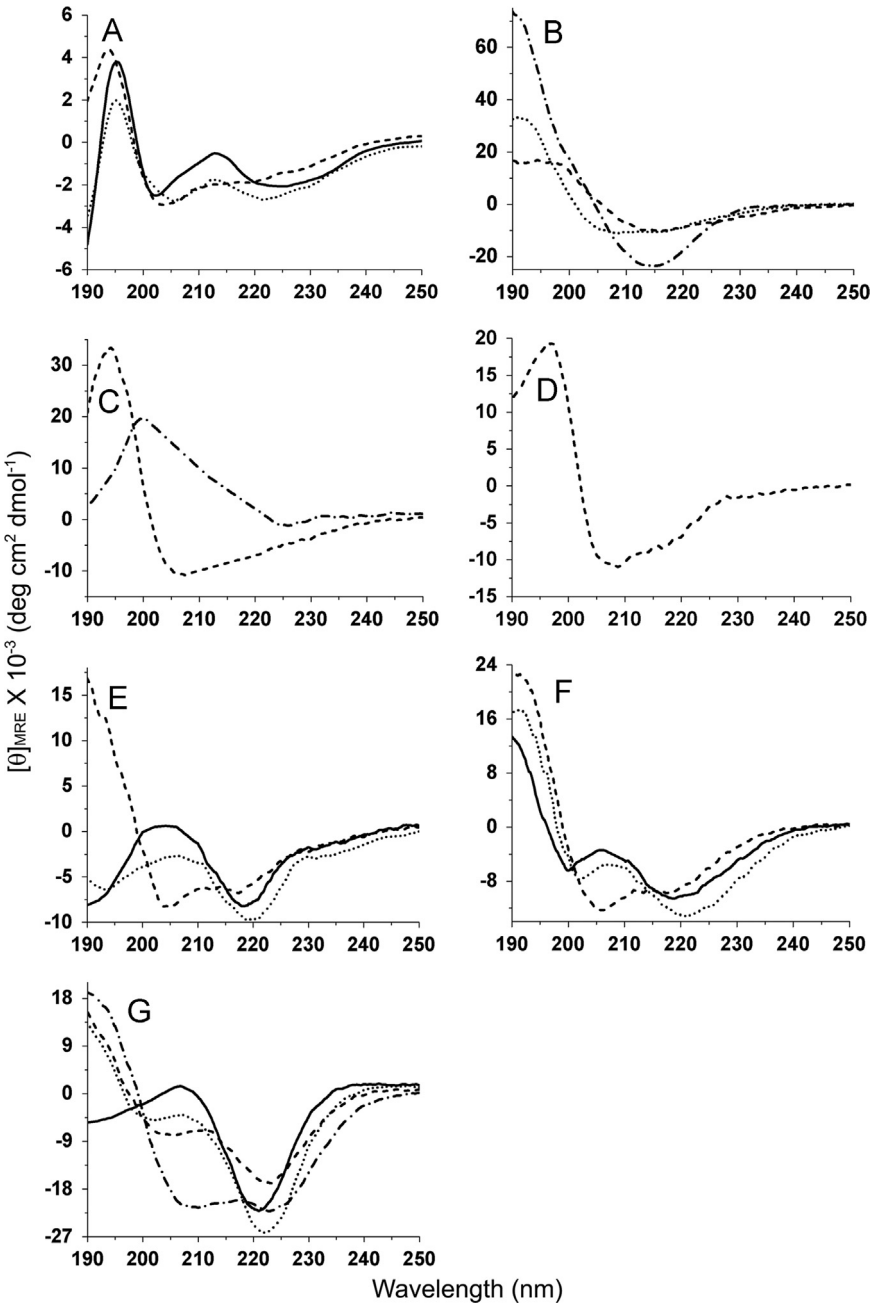


**Fig. 6.** CD spectra of the peptides recorded in fluorinated alcohols (HFIP and TFE, continuous and dotted lines, respectively) and their aqueous mixtures (20% HFIP and 20% TFE, dashed and dash-dotted lines, respectively). Panels A–G represent the spectra recorded for the peptides AβFF, AβFY, AβYF, AβYY, AβYW, AβWY, and AβWW, respectively.

in amide I region centered around 1629 $cm^{-1}$ upon drying from HFIP stock whereas peptide solutions dried from TFE, 20% HFIP, and 20% TFE are centered around 1626 $cm^{-1}$ (Panel C). AβYY structures from HFIP exhibit an amide band centered at 1631 $cm^{-1}$ whereas structures from other conditions show bands centered around 1627 $cm^{-1}$ (Panel D). Peptide AβYW shows sharp peaks in amide I region centered at ~1625–1628 upon drying from HFIP, 20% HFIP, TFE, and 20% TFE (Panel E). AβWY shows sharp peaks in amide I region centered at 1630 $cm^{-1}$ upon drying from HFIP, 20% HFIP, TFE, and 20% TFE, indicating predominant β-structure (Panel F). AβWW shows peaks centered in the range of 1627–1630 $cm^{-1}$ upon drying from HFIP, 20% HFIP, TFE, and 20% TFE. β-structure from all conditions of dissolution is clearly evident. A prominent band at about 1668 $cm^{-1}$ indicating β-turn conformation is evident from HFIP and 20% HFIP. Significant intensity at 1685–1695 $cm^{-1}$ in almost all the spectra could be attributed to the presence of non-fibrillar structures or antiparallel β-sheet structure [54,55]. This data suggest that the structures from all the peptides adopt predominantly β-structure in dry form irrespective of their solvent history. Subtle differences in spectra can be attributed to the differences in the intermolecular hydrogen bond strengths and presence non-fibrillar structures.

## 4. Discussion

Aromatic interactions play an important role in stabilizing tertiary and quaternary structure of proteins [1,2,7]. The preferred parallel displaced π-stacking interactions are more stable than the T-shaped interactions in isolated dimer pairs of aromatic residues in proteins [56]. Most of the studies on amyloidogenic peptides

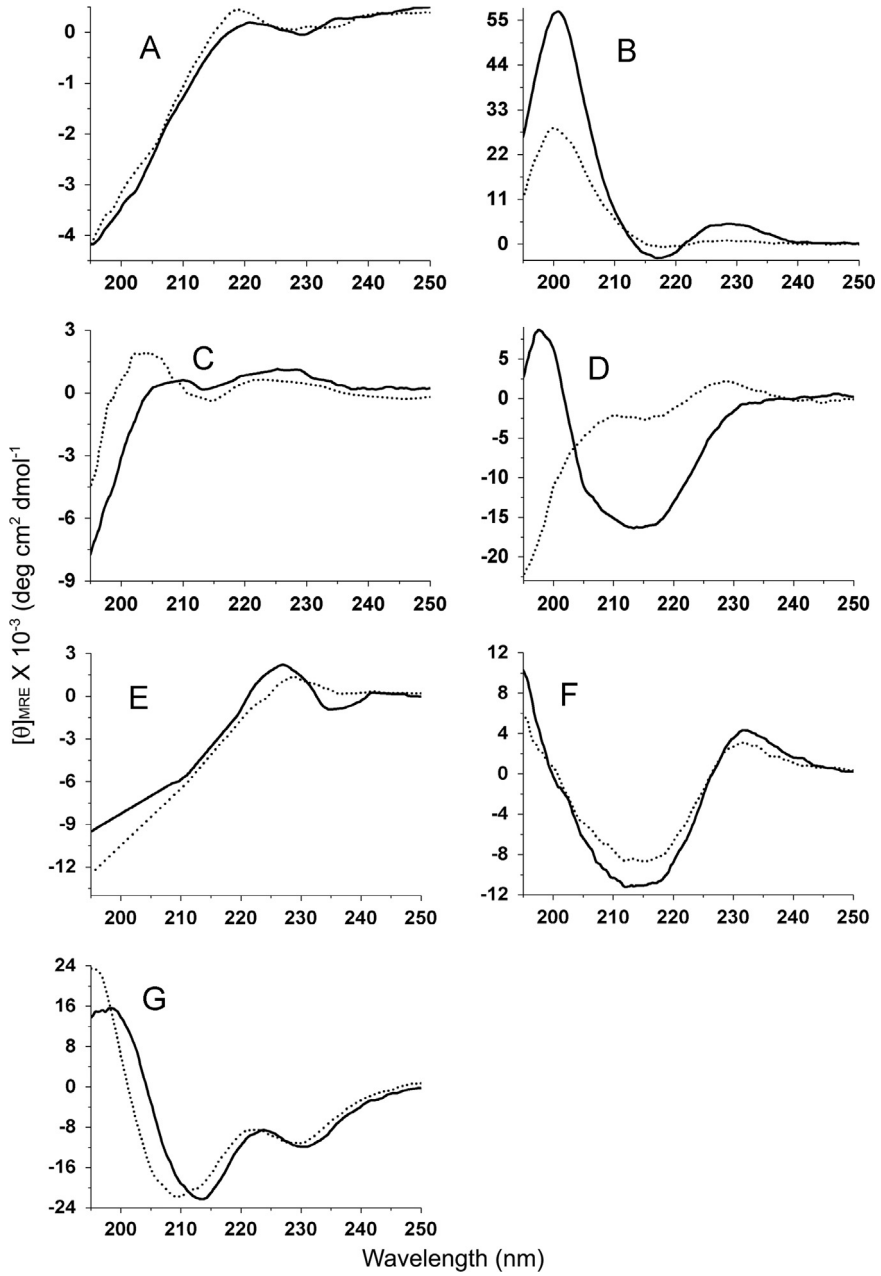


**Fig. 7.** CD spectra of the peptides in deionised water upon direct dissolution of peptides (continuous line) and dissolution after DMSO treatment (dotted line). Panels A–G represent the spectra recorded for the peptides AβFF, AβFY, AβYF, AβYY, AβYW, AβWY, and AβWW, respectively.

and proteins have highlighted the role of F [57,58], but only few of them discussed the relative preference of F, Y and W in amyloid fibril formation. An appropriate combination of several non-covalent interactions such as aromatic stacking, hydrogen bonding, hydrophobic, electrostatic and van der Walls interactions or even steric interactions are responsible for amyloid formation [45,59–62]. Analogs of Aβ(16–22) peptide have been studied particularly where the F residues have been substituted with F derivatives and other hydrophobic residues [59,60,63]. The results suggested that peptide sequence, secondary structure propensity, aromatic, hydrophobic, and steric considerations play important role in fibril formation. Although a large number of Aβ40 and Aβ42 variants and their fragments have been synthesized, both the F residues have not been replaced by Y or W. To get insights into the relative preference of F, Y, and W in amyloid fibril formation and their positional preference in the Aβ(16–22) sequence, analogs wherein F was substituted with Y and W were synthesized and their aggregation behaviour examined from fluorinated alcohols (HFIP and TFE) and their aqueous mixtures (20% HFIP or TFE in deionized water) under organic solvent cluster forming conditions. Aggregation of peptides in deionized water after direct dissolution and dissolution after DMSO treatment was also examined.

Imaging by AFM shows very different morphologies of aggregates depending on the solvent from which peptides were dried. Results suggest that fibrillar morphology is more pronounced from TFE as compared to HFIP in the case of AβFY, AβYF and AβYY peptides. Though solvent dependent morphological differences are evident, fibrillar structures are not observed for AβFF. All the tryptophan containing peptides (AβYW, AβWY and AβWW) formed ring-like structures from HFIP solutions whereas polymorphic structures were evident from the TFE. The morphology of aggregates does not appear to be dependent on the conformation of

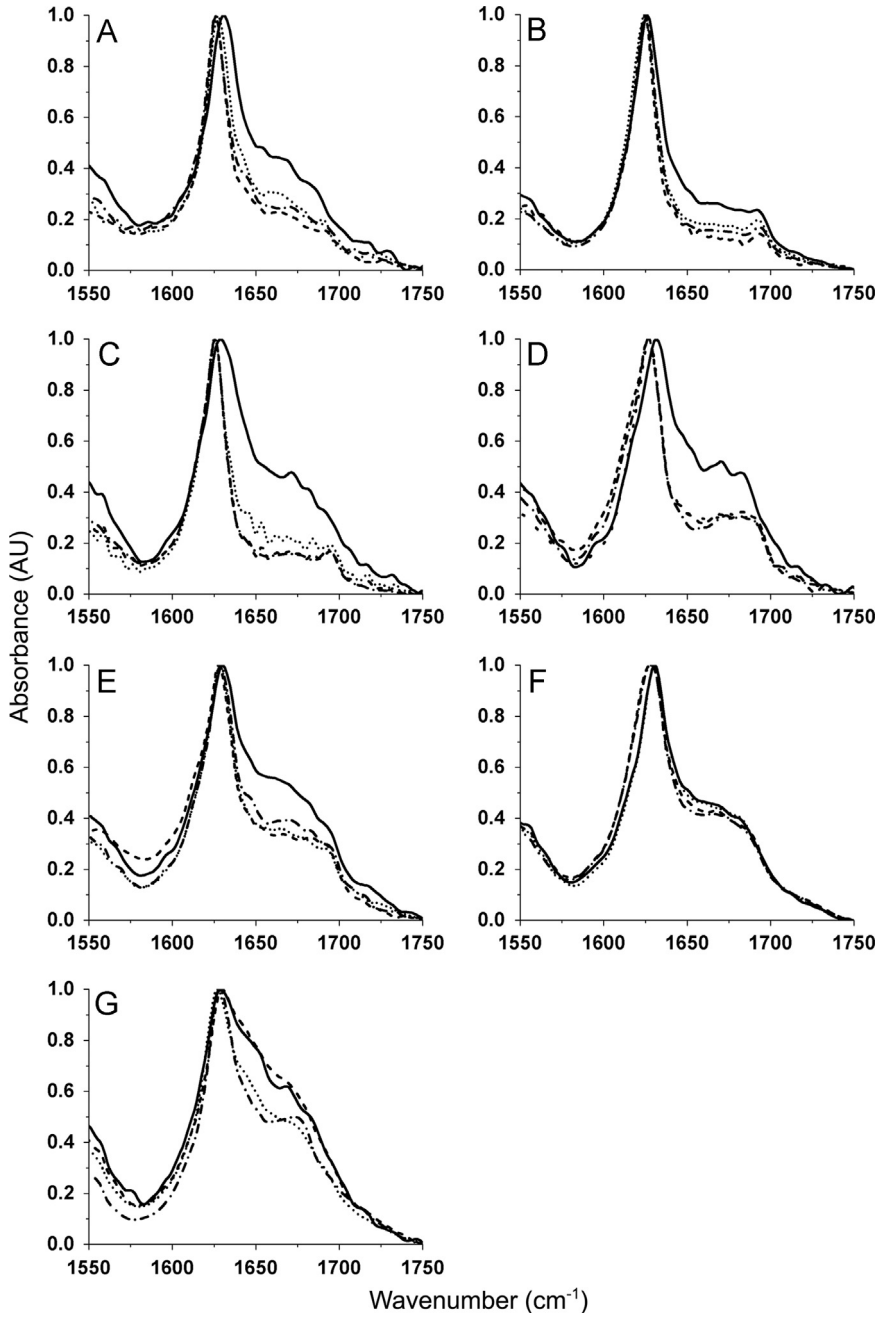


**Fig. 8.** FTIR spectra of the peptides recorded in solid state after drying the peptides from fluorinated alcohols (HFIP and TFE, continuous and dotted lines, respectively) and their aqueous mixtures (20% HFIP and 20% TFE, dashed and dash-dotted lines, respectively). Panels A–G represent the spectra recorded for the peptides AβFF, AβFY, AβYF, AβYY, AβYW, AβWY, and AβWW, respectively.

peptides in solution or in the solid state except for AβFY and AβWW. AβFY adopts unordered and β-structure in HFIP and TFE, respectively which is also reflected in the structures imaged by AFM, as the distinct fibrillar structures were formed from TFE and amorphous aggregates from HFIP irrespective of peptide conformation in solid state. AβWW adopts unordered conformation in both the solvents but the conformations in solid state are different. The rapid evaporation of alcohols on the mica surface would result in favourable hydrophobic interactions and interactions between the aromatic side-chains which can drive the self-assembly of structures. In neat fluorinated organic solvents such as TFE and HFIP, the replacement of hydration shell by alcohol molecules followed by hydrogen bonds can induce secondary structures such as helix or β-hairpin [31,32,64]. We have earlier shown that the ordered ring-like structures are formed upon drying of Aβ(16–22). and Aβ peptides (Aβ40, Aβ42 and Aβ43) from HFIP [41]. Structures observed from HFIP and TFE (except AβFY in TFE) could be similar to intermolecular molten particles where the peptide molecules are not organized into cross-β structures [40] unlike ordered ring-like structures [41].

Aqueous mixtures of HFIP and TFE are known to modulate formation of amyloid fibrils under solvent cluster forming conditions [26,27,30,33–35]. The fibrillar morphologies were more prominent from 20% TFE but the aggregates formed in 20% HFIP showed relatively more intense ThT fluorescence from all the peptides except AβFF. It suggests that cluster forming conditions from HFIP favours amyloid formation as compared to TFE when F is replaced with less hydrophobic aromatic residues. Cluster forming conditions are more

favourable for hydrophobic interactions of peptide side-chains as compared to neat solvents and might favour formation of cross-β aggregates. Our results clearly indicate that the morphology and amyloid nature of aggregates formed in aqueous HFIP are dependent on the sequence of aromatic residues. Fibrils (indicating predominance of cross-β structure) observed only in case of AβFY and AβWW. Twisted ribbons were observed earlier for Aβ(13–21) K16A peptide [65]. Assembly of nanotubes via twisted and helical ribbon intermediates has been reported for AβFF under acidic condition [40,66]. Non-amyloid twisted tape-like structures at acidic pH and untwisted tape-like structures at basic pH has also been reported for AβFF [45]. Our results indicate that the ribbon-like structures could be both amyloid (AβYF from aqueous TFE and aqueous HFIP) and non-amyloid (AβYW from aqueous TFE) in nature. Moreover, further assembly of ribbon-like structures can result in to fibrillar structures of either amyloid (AβFY from aqueous TFE) or non-amyloid nature (AβWY from aqueous TFE).

The dissolution of peptides in DMSO followed by drying and dissolution in water leads to significant differences in the self-assembly as compared to the peptides dissolved in water directly. The difference in the morphology of self-assembled structures and their cross-β nature is more pronounced in the F and Y containing peptides as compared to those having W19, W20, or both the residues. All the peptides having same aromatic residue at both 19th and 20th position formed amyloid fibrils in water indicating the role of same aromatic residue at both the positions for amyloid fibril formation. Moreover, AβYY form amyloid fibrils showing highest ThT fluorescence intensity as compared to the fibrils formed by other peptides in water despite the least hydrophobic nature of Y side-chains. The modulation of self-assembly by DMSO treatment may be attributed to the dissociation low molecular weight of oligomers that might be present in HPLC purified peptide.

The importance of F19 is crucial in the self-assembly of AβFF because of possible π–π stacking of the F side-chains establishing inter-strand contacts as reported earlier [60,63,67]. The ability of AβFW to form amyloid fibrils but not AβWF indicates the importance of F19 residue in amyloid fibril formation [68]. In this case, stacking of F side-chains at 19th position is possible for both AβFF and AβFY whereas stacking between Y side-chains can take place for AβYF, AβYY and AβYW. W19 side-chains can stack in AβWY and AβWW peptides. The stacking between F–F, Y–Y and W–W may not be the same because lone electron pair of the OH group can conjugate to the aromatic ring in case of Y and W side-chains are significantly bulkier than both F and Y. The difference in the electronic state of aromatic ring of Y could lead to T-shaped geometry of aromatic rings as opposed to edge to face or parallel geometry of F side-chains [6,58,67,69]. T-shaped interactions could possibly lead to exposure of hydrophobic surfaces. The exposed hydrophobic surfaces can possibly be buried effectively by twisting of the structures [70] as observed in case of AβYF structures formed under cluster forming conditions. The hydrophobic surfaces could also favour supra-assembly of initial assemblies for their effective burial as in case of AβYY in 20% HFIP. Propensities of AβFY and AβWW to form amyloid fibrils can be attributed to formation of β-structure in solution. Morphological differences in the structures under different solvent conditions can be attributed to different packing of β-strands or sheets, and inter-strand and inter-sheet side-chain contacts. Amyloid fibril formation is also dependent on the solvent conditions. Amyloid forming propensity of AβFY is significantly less in water as compared to aqueous mixtures of fluorinated alcohols. AβYY showed more amyloid forming propensity in water and less in aqueous mixtures of fluorinated alcohols as opposed to AβFY. There is no significant difference in the propensities of amyloid formation of W containing peptides and AβYF. The results indicate that not only the aromatic residue at 19th position but also at 20th position plays an important role in the self-assembly and amyloid nature of aggregates.

## 5. Conclusions

The results described in this paper indicate that the replacement of F by Y and W in Aβ(16–22) sequence clearly modulates amyloid fibril formation, as fibrillar structures of varying morphologies and cross-β structure content were observed. Formation of structures of different morphologies and varying cross-β structure depends upon the solvent conditions, aromatic residues and their positions in the peptide sequence. This could arise due to different strengths of stacking of aromatic side-chains or their packing which could result to different packing of β-strands or sheets, and inter-strand and inter-sheet side-chain contacts.

## Acknowledgements

Help from A Harikrishna in recording TEM images is acknowledged. Funding from CSIR Network Project BSC 0112 is gratefully acknowledged. RN is the recipient of JC Bose Fellowship from the Department of Science and Technology, India.

## Appendix A. Transparency document

Supplementary data associated with this article can be found in the online version at http://dx.doi.org/10.1016/j.bbrep.2015.04.005.

## References

[1] S.K. Burley, G.A. Petsko, Aromatic–aromatic interaction: a mechanism of protein structure stabilization, Science 229 (1985) 23–28.
[2] L. Serrano, M. Bycroft, A.R. Fersht, Aromatic–aromatic interactions and protein stability: investigation by double-mutant cycles, J. Mol. Biol. 218 (1991) 465–475.
[3] R.M. Johnson, K. Hecht, C.M. Deber, Aromatic and cation–π interactions enhance helix–helix association in a membrane environment, Biochemistry 46 (2007) 9208–9214.
[4] L.A. Eidenschink, B.L. Kier, N.H. Andersen, Determinants of Fold Stabilizing Aromatic–Aromatic Interactions in Short Peptides, Adv. Exp. Med. Biol. 611 (2009) 73–74.
[5] L.M. Espinoza-Fonseca, J. García-Machorro, Aromatic–aromatic interactions in the formation of the MDM2–p53 complex, Biochem. Biophys. Res. Commun. 370 (2008) 547–551.
[6] R. Chelli, F.L. Gervasio, P. Procacci, V. Schettino, Stacking and T-shape competition in aromatic–aromatic amino acid interactions, J. Am. Chem. Soc. 124 (2002) 6133–6143.
[7] E. Lanzarotti, R.R. Biekofsky, D.A. Estrin, M.A. Marti, A.G. Turjanski, Aromatic–aromatic interactions in proteins: beyond the dimer, J. Chem. Inf. Model. 51 (2011) 1623–1633.
[8] A. Thomas, R. Meurisse, B. Charloteaux, R. Brasseur, Aromatic side-chain interactions in proteins I. Main structural features, Proteins: Struct. Funct. Bioinf. 48 (2002) 628–634.
[9] C.D. Tatko, M.L. Waters, Selective aromatic interactions in β-hairpin peptides, J. Am. Chem. Soc. 124 (2002) 9372–9373.
[10] L. Wu, D. McElheny, T. Takekiyo, T.A. Keiderling, Geometry and efficacy of cross-strand Trp/Trp, Trp/Tyr, and Tyr/Tyr aromatic interaction in a β-hairpin peptide, Biochemistry 49 (2010) 4705–4714.
[11] T. Takekiyo, L. Wu, Y. Yoshimura, A. Shimizu, T.A. Keiderling, Relationship between hydrophobic interactions and secondary structure stability for trpzip β-hairpin peptides, Biochemistry 48 (2009) 1543–1552.
[12] R. Azriel, E. Gazit, Analysis of the minimal amyloid-forming fragment of the islet amyloid polypeptide. An experimental support for the key role of the phenylalanine residue in amyloid formation, J. Biol. Chem. 276 (2001) 34156–34161.
[13] B. Haggqvist, J. Naslund, K. Sletten, G.T. Westermark, G. Mucchiano, L.O. Tjernberg, C. Nordstedt, U. Engstrom, P. Westermark, Medin: an integral fragment of aortic smooth muscle cell-produced lactadherin forms the most common human amyloid, Proc. Natl. Acad. Sci. USA 96 (1999) 8669–8674.
[14] S. Jones, J. Manning, N.M. Kad, S.E. Radford, Amyloid-forming peptides from $\beta_2$-microglobulin-insights into the mechanism of fibril formation *in vitro*, J. Mol. Biol. 325 (2003) 249–257.
[15] M. Reches, Y. Porat, E. Gazit, Amyloid fibril formation by pentapeptide and tetrapeptide fragments of human calcitonin, J. Biol. Chem. 277 (2002) 35475–35480.
[16] G.T. Westermark, U. Engstrom, P. Westermark, The N-terminal segment of protein AA determines its fibrillogenic property, Biochem. Biophys. Res. Commun. 182 (1992) 27–33.

[17] E. Gazit, Self-assembled peptide nanostructures: the design of molecular building blocks and their technological utilization, Chem. Soc. Rev. 36 (2007) 1263–1269.
[18] Y. Porat, Y. Mazor, S. Efrat, E. Gazit, Inhibition of islet amyloid polypeptide fibril formation: a potential role for heteroaromatic interactions, Biochemistry 43 (2004) 14454–14462.
[19] K.N.L. Huggins, M. Bisaglia, L. Bubacco, M. Tatarek-Nossol, A. Kapurniotu, N.H. Andersen, Designed hairpin peptides interfere with amyloidogenesis pathways: fibril formation and cytotoxicity inhibition, interception of the preamyloid state, Biochemistry 50 (2011) 8202–8212.
[20] D.J. Gordon, K.L. Sciarretta, S.C. Meredith, Inhibition of β-amyloid(40) fibrillogenesis and disassembly of β-amyloid(40) fibrils by short β-amyloid congeners containing N-methyl amino acids at alternate residues, Biochemistry 40 (2001) 8237–8245.
[21] W.B. Stine Jr., K.N. Dahlgren, G.A. Krafft, M.J. LaDu, *In vitro* characterization of conditions for amyloid-β peptide oligomerization and fibrillogenesis, J. Biol. Chem. 278 (2003) 11612–11622.
[22] X. Dai, Y. Sun, Z. Gao, Z. Jiang, Copper enhances amyloid-β peptide neurotoxicity and non β-aggregation: a series of experiments conducted upon copper-bound and copper-free amyloid-β peptide, J. Mol. Neurosci. 41 (2010) 66–73.
[23] C. Avidan-Shpalter, E. Gazit, The early stages of amyloid formation: biophysical and structural characterization of human calcitonin pre-fibrillar assemblies, Amyloid 13 (2006) 216–225.
[24] A. Hirata, K. Sugimoto, T. Konno, T. Morii, Amyloid-forming propensity of the hydrophobic non-natural amino acid on the fibril-forming core peptide of human tau, Bioorg. Med. Chem. Lett. 17 (2007) 2971–2974.
[25] P. Marek, A. Abedini, B. Song, M. Kanungo, M.E. Johnson, R. Gupta, W. Zaman, S.S. Wong, D.P. Raleigh, Aromatic interactions are not required for amyloid fibril formation by islet amyloid polypeptide but do influence the rate of fibril formation and fibril morphology, Biochemistry 46 (2007) 3255–3261.
[26] M.R. Nichols, M.A. Moss, D.K. Reed, S. Cratic-McDaniel, J.H. Hoh, T.L. Rosenberry, Amyloid-β protofibrils differ from amyloid-β aggregates induced in dilute hexafluoroisopropanol in stability and morphology, J. Biol. Chem. 280 (2005) 2471–2480.
[27] K. Yamaguchi, H. Naiki, Y. Goto, Mechanism by which the amyloid-like fibrils of a $\beta_2$-microglobulin fragment are induced by fluorine-substituted alcohols J. Mol. Biol. 363 (2006) 279–288.
[28] S.B. Padrick, A.D. Miranker, Islet amyloid: a phase partitioning and secondary nucleation are central to the mechanism of fibrillogenesis, Biochemistry 41 (2002) 4694–4703.
[29] H. Muta, Y.-H. Lee, J.z. Kardos, Y. Lin, H. Yagi, Y. Goto, Supersaturation-limited amyloid fibrillation of insulin revealed by ultrasonication, J. Biol. Chem. 289 (2014) 18228–18238.
[30] S. Lesné, M.T. Koh, L. Kotilinek, R. Kayed, C.G. Glabe, A. Yang, M. Gallagher, K.H. Ashe, A specific amyloid-β protein assembly in the brain impairs memory, Nature 440 (2006) 352–357.
[31] M. Buck, Trifluoroethanol and colleagues: cosolvents come of age. Recent studies with peptides and proteins, Q. Rev. Biophys. 31 (1998) 297–355.
[32] R. Rajan, P. Balaram, A model for the interaction of trifluoroethanol with peptides and proteins, Int. J. Pept. Protein Res. 48 (1996) 328–336.
[33] V.L. Anderson, T.F. Ramlall, C.C. Rospigliosi, W.W. Webb, D. Eliezer, Identification of a helical intermediate in trifluoroethanol-induced α-synuclein aggregation, Proc. Natl. Acad. Sci. 107 (2010) 18850–18855.
[34] Y. Fezoui, D.B. Teplow, Kinetic studies of amyloid β-protein fibril assembly. Differential effects of α-helix stabilization, J. Biol. Chem. 277 (2002) 36948–36954.
[35] T. Kanno, K. Yamaguchi, H. Naiki, Y. Goto, T. Kawai, Association of thin filaments into thick filaments revealing the structural hierarchy of amyloid fibrils, J. Struct. Biol. 149 (2005) 213–218.
[36] E. Atherton, Solid Phase Synthesis: A Practical Approach, IRL Press, Oxford, 1989.
[37] J.M. Stewart, J.D. Young, Solid Phase Peptide Synthesis, Pierce Chemical Company Rockford, IL, 1984.
[38] D.S. King, C.G. Fields, G.B. Fields, A cleavage method which minimizes side reactions following Fmoc solid phase peptide synthesis, Int. J. Pept. Protein Res. 36 (1990) 255–266.
[39] I. Horcas, R. Fernández, J.M. Gómez-Rodríguez, J. Colchero, J. Gómez-Herrero, A.M. Baro, WSXM: a software for scanning probe microscopy and a tool for nanotechnology, Rev. Sci. Instrum. 78 (2007) 013705.
[40] W.S. Childers, N.R. Anthony, A.K. Mehta, K.M. Berland, D.G. Lynn, Phase networks of cross-β peptide assemblies, Langmuir 28 (2012) 6386–6395.
[41] S.K. Pachahara, N. Chaudhary, C. Subbalakshmi, R. Nagaraj, Hexafluoroisopropanol induces self-assembly of β-amyloid peptides into highly ordered nanostructures, J. Pept. Sci. 18 (2012) 233–241.
[42] V. Castelletto, I.W. Hamley, C. Cenker, U. Olsson, Influence of salt on the self-assembly of two model amyloid heptapeptides, J. Phys. Chem. B 114 (2010) 8002–8008.
[43] M. Gupta, A. Bagaria, A. Mishra, P. Mathur, A. Basu, S. Ramakumar, V.S. Chauhan, Self-assembly of a dipeptide-containing conformationally restricted dehydrophenylalanine residue to form ordered nanotubes, Adv. Mater. 19 (2007) 858–861.
[44] M.J. Krysmann, V. Castelletto, A. Kelarakis, I.W. Hamley, R.A. Hule, D.J. Pochan, Self-assembly and hydrogelation of an amyloid peptide fragment, Biochemistry 47 (2008) 4597–4605.
[45] K. Tao, J. Wang, P. Zhou, C. Wang, H. Xu, X. Zhao, J.R. Lu, Self-assembly of short Aβ(16–22) peptides: effect of terminal capping and the role of electrostatic interaction, Langmuir 27 (2011) 2723–2730.
[46] R.W. Woody, Contributions of tryptophan side chains to the far-ultraviolet circular dichroism of proteins, Eur. Biophys. J. 23 (1994) 253–262.
[47] R.W. Woody, Circular dichroism, Methods Enzymol. 246 (1995) 34–71.
[48] V. Pak, M. Koo, D. Kwon, L. Yun, Design of a highly potent inhibitory peptide acting as a competitive inhibitor of HMG-CoA reductase, Amino Acids 43 (2012) 2015–2025.
[49] J. Engel, E. Liehl, C. Sorg, Circular dichroism, optical rotatory dispersion and helix–coil transition of polytyrosine and tyrosine peptides in non-aqueous solvents, Eur. J. Biochem. 21 (1971) 22–30.
[50] I.W. Hamley, V. Castelletto, C. Moulton, D. Myatt, G. Siligardi, C.L.P. Oliveira, J.S. Pedersen, I. Abutbul, D. Danino, Self-assembly of a modified amyloid peptide fragment: pH-responsiveness and nematic phase formation, Macromol. Biosci. 10 (2010) 40–48.
[51] A.S. Ladokhin, M.E. Selsted, S.H. White, CD spectra of indolicidin antimicrobial peptides suggest turns, not polyproline helix, Biochemistry 38 (1999) 12313–12319.
[52] S. Choi, W. Jeong, S.K. Kang, M. Lee, E. Kim, D.Y. Ryu, Y. Lim, Differential self-assembly behaviors of cyclic and linear peptides, Biomacromolecules 13 (2012) 1991–1995.
[53] W.K. Surewicz, H.H. Mantsch, D. Chapman, Determination of protein secondary structure by fourier transform infrared spectroscopy: a critical assessment, Biochemistry 32 (1993) 389–394.
[54] R. Sarroukh, E. Goormaghtigh, J.M. Ruysschaert, V. Raussens, ATR-FTIR: a rejuvenated tool to investigate amyloid proteins, Biochim. Biophys. Acta-Biomembr. 1828 (2013) 2328–2338.
[55] K. Bagińska, J. Makowska, W. Wiczk, F. Kasprzykowski, L. ChmurzyńSki, Conformational studies of alanine-rich peptide using CD and FTIR spectroscopy, J. Pept. Sci. 14 (2008) 283–289.
[56] G.B. McGaughey, M. Gagne, A.K. Rappe, π-Stacking interactions. Alive and well in proteins, J. Biol. Chem. 273 (1998) 15458–15463.
[57] J. Naskar, M.G.B. Drew, I. Deb, S. Das, A. Banerjee, Water-soluble tripeptide Aβ (9–11) forms amyloid-like fibrils and exhibits neurotoxicity, Org. Lett. 10 (2008) 2625–2628.
[58] Y. Porat, A. Stepensky, F.X. Ding, F. Naider, E. Gazit, Completely different amyloidogenic potential of nearly identical peptide fragments, Biopolymers 69 (2003) 161–164.
[59] F.T. Senguen, T.M. Doran, E.A. Anderson, B.L. Nilsson, Clarifying the influence of core amino acid hydrophobicity, secondary structure propensity, and molecular volume on amyloid-β 16-22 self-assembly, Mol. BioSyst. 7 (2011) 497–510.
[60] F.T. Senguen, N.R. Lee, X. Gu, D.M. Ryan, T.M. Doran, E.A. Anderson, B.L. Nilsson, Probing aromatic, hydrophobic, and steric effects on the self-assembly of an amyloid-β fragment peptide, Mol. BioSyst. 7 (2011) 486–496.
[61] J. Park, B. Kahng, W. Hwang, Thermodynamic selection of steric zipper patterns in the Amyloid Cross-β Spine, PLoS Comput. Biol. 5 (2009) e1000492.
[62] A.T. Petkova, G. Buntkowsky, F. Dyda, R.D. Leapman, W.M. Yau, R. Tycko, Solid state NMR reveals a pH-dependent antiparallel β-sheet registry in fibrils formed by a β-amyloid peptide, J. Mol. Biol. 335 (2004) 247–260.
[63] H. Inouye, K.A. Gleason, D. Zhang, S.M. Decatur, D.A. Kirschner, Differential effects of phe19 and phe20 on fibril formation by amyloidogenic peptide Aβ 16–22 (Ac-KLVFFAE-NH2), Proteins: Sruct. Funct. Bioinf. 78 (2010) 2306–2321.
[64] F.J. Blanco, M.A. Jimenez, A. Pineda, M. Rico, J. Santoro, J.L. Nieto, NMR solution structure of the isolated N-terminal fragment of protein-G B1 Domain. Evidence of trifluoroethanol induced native-like β-hairpin formation, Biochemistry 33 (1994) 6004–6014.
[65] J. Dong, K. Lu, A. Lakdawala, A.K. Mehta, D.G. Lynn, Controlling amyloid growth in multiple dimensions, Amyloid 13 (2006) 206–215.
[66] K. Lu, J. Jacob, P. Thiyagarajan, V.P. Conticello, D.G. Lynn, Exploiting amyloid fibril lamination for nanotube self-assembly, J. Am. Chem. Soc. 125 (2003) 6391–6393.
[67] A.K. Mehta, K. Lu, W.S. Childers, Y. Liang, S.N. Dublin, J. Dong, J.P. Snyder, S.V. Pingali, P. Thiyagarajan, D.G. Lynn, Facial symmetry in protein self-assembly, J. Am. Chem. Soc. 130 (2008) 9829–9835.
[68] N. Chaudhary, R. Nagaraj, Impact on the replacement of phe by trp in a short fragment of Aβ amyloid peptide on the formation of fibrils, J. Pept. Sci. 17 (2011) 115–123.
[69] A.A. Profit, V. Felsen, J. Chinwong, E.R.E. Mojica, R.Z.B. Desamero, Evidence of π-stacking interactions in the self-assembly of hIAPP22-29, Proteins: Struct. Funct. Bioinf 81 (2013) 690–703.
[70] M. Bouchard, J. Zurdo, E.J. Nettleton, C.M. Dobson, C.V. Robinson, Formation of insulin amyloid fibrils followed by FTIR simultaneously with CD and electron microscopy, Protein Sci. 9 (2000) 1960–1967.